Applied Catalysis B: Environmental 148–149 (2014) 557–567

Contents lists available at ScienceDirect

Applied Catalysis B: Environmental

journal homepage: www.elsevier.com/locate/apcatb

Microwave heated synthesis of carbon supported Pd, Ni and Pd–Ni nanoparticles for methanol oxidation in KOH solution

R.S. Amin[a], R.M. Abdel Hameed[b,*], K.M. El–Khatib[a]

[a] Chemical Engineering & Pilot Plant Department, National Research Center, Dokki, Giza, Egypt
[b] Chemistry Department, Faculty of Science, Cairo University, Giza, Egypt

ARTICLE INFO

Article history:
Received 8 September 2013
Received in revised form
11 November 2013
Accepted 13 November 2013
Available online 1 December 2013

Keywords:
Methanol
Alkaline medium
Nickel
Palladium
Carbon

ABSTRACT

Pd, Ni and Pd–Ni nanoparticles uniformly dispersed on Vulcan XC-72R carbon black are prepared by microwave-irradiation using $NaBH_4$ as a reducing agent. Pd/C, Ni/C and Pd–Ni/C electrocatalysts were characterized by X-ray diffraction (XRD), transmission electron microscopy (TEM) and energy-dispersive X-ray spectroscopy (EDX). Pd–Ni alloy was formed with an average particle size of 3 nm. Kinetic parameters such as the electron transfer coefficient value (α) and electron transfer rate constant of Ni/C and Pd–Ni/C electrocatalysts in 0.5 M KOH solution were calculated. The prepared electrocatalysts were examined for methanol oxidation in alkaline medium. The long-term stability of electrocatalysts in (0.6 M MeOH + 0.5 M KOH) solution was studied using repeated cyclic voltammetry and chronoamperometry. Two methanol oxidation peaks were observed at Pd–Ni/C at 0 and +913 mV. Their current density values are higher than those at Pd/C and Ni/C electrocatalysts by 3.84 and 1.43 times, respectively. The catalytic rate constant at Ni/C and Pd–Ni/C was estimated using double-step chronoamperometry as 1.80×10^3 and 5.88×10^3 cm^3 mol^{-1} s^{-1}, respectively. Pd–Ni/C showed better stability performance when compared to Pd/C and Ni/C electrocatalysts.

1. Introduction

Direct methanol fuel cells (DMFCs) are a special form of low-temperature polymer electrolyte membrane fuel cells technology. Electric power is produced by direct conversion of liquid methanol (no need of hydrogen) to hydrogen ions on the anode side of the fuel cell. High energy density, quick start-up and avoiding membrane humidification problems are the major advantages of DMFC. However, it suffers from the poor kinetics of methanol oxidation reaction, significant fuel crossover and safety concerns [1].

Electrocatalysts based on Pt nanoparticles showed high electrocatalytic activity towards methanol oxidation [2,3]. However, their high cost and susceptibility to be poisoned by CO-like intermediates formed during methanol oxidation are the main drawbacks that can hinder the commercialization of DMFC technology [4]. Therefore, the development of non-platinum electrocatalysts with comparable activity to those based on platinum is a key step on the road to DMFCs marketing. Generally, If DMFCs operate in an alkaline, instead of an acidic electrolyte, the kinetics would be significantly improved and Pt-free electrocatalysts can be then used.

Recently, many alternative metals to platinum have been investigated [4–7]. Pd represents a promising low cost electrocatalyst with high catalytic activity towards alcohol oxidation in alkaline media [8–14]. It is also more abundant in earth than Pt by about 50 times [15]. Pd is very stable in acidic fuel cell environment [16] and showed good electrocatalytic properties for CO electrooxidation during methanol, ethanol [8,9,17,18] and formic acid [19–22] electrooxidation. Alloying Pd with other metals like Ni [4,5,23–26] and Co [2,10] could further enhance its reactivity for methanol oxidation in alkaline medium.

The catalytic activity of an electrocatalyst depends on its particle size distribution and dispersion on the carbon support [27]. An enhanced electrocatalytic performance was gained at catalyst particles in nanometer size with narrow size distribution. This could be controlled via the synthesis procedure [28,29]. Various approaches were adopted to prepare supported catalysts, such as wet impregnation [30], ion exchange [31], physical deposition [32] and colloidal methods [33]. In the impregnation method, the metal precursor salt should be reduced in hydrogen atmosphere at high temperature [34]. This applied heat treatment resulted in an increased particle size, thus reducing the catalytic activity of the formed electrocatalyst [35,36]. On the other hand, colloidal procedure consists of many steps with repeated filtering and washing. Therefore, a lower yield would be obtained with a higher overall catalyst production cost.

* Corresponding author. Tel.: +201145565646; fax: +235727556.
E-mail addresses: randa311eg@yahoo.com, noura31176@hotmail.com (R.M.A. Hameed).

0926-3373/$ – see front matter © 2013 Elsevier B.V. All rights reserved.
http://dx.doi.org/10.1016/j.apcatb.2013.11.020

Pd–Ni alloy catalysts were prepared by different methods to act as anode materials for methanol oxidation in alkaline medium. They were supported on Vulcan XC-72 carbon by chemical reduction with formic acid [4]. Nanocrystalline $Pd_{40}Ni_{60}$ catalyst has been fabricated by dealloying a ternary $Al_{75}Pd_{10}Ni_{15}$ alloy in a 20 wt% NaOH solution under free corrosion conditions. It showed an enhanced electrocatalytic performance towards methanol oxidation than nanoporous Pd did [23]. Pd–Ni nanoparticles were also produced by electroless plating onto the inner side-walls of three-dimensional silicon microchannel plates and followed by annealing at 300 °C under argon. Methanol oxidation onset potential at these composites was shifted in the negative direction with a stabilized current response during long-term cyclization [24]. The introduction of Ni to active Pd–1 wt% MWCNTs electrode increased its apparent electrocatalytic activity by 1.4–1.7 times [25]. On the other hand, a better stability was observed at core/shell Ni@Pd nanoparticles supported on MWCNTs [5]. This may be ascribed to their improved geometrical as well as electronic properties.

To the best of our knowledge, carbon supported Pd–Ni nanoparticles are prepared in this study for the first time using a simple household microwave oven as a heating source and $NaBH_4$ as a reducing agent. This offers a simple and rapid synthesis method for metal nanoparticles [37]. It could uniformly transfer heat to the substance through the microwave-transparent reaction container (i.e., glass or plastic). This results in a more homogeneous nucleation of catalyst nanoparticles and shorter crystallization time in relation to other conventional heating methods. In these methods, temperature gradients could not be avoided, leading to an adverse effect on the particle size distribution and yield. Pd–Ni alloy nanoparticles will be further characterized by XRD, TEM and EDX. The electrocatalytic activity of the prepared catalysts is studied in 0.5 M KOH solution using cyclic voltammetry and chronoamperometry techniques. Pd/C and Ni/C electrocatalysts are also prepared under the same conditions for comparison.

2. Experimental

2.1. Chemicals

Carbon-supported Pd (Pd/C), Ni (Ni/C) and Pd–Ni (Pd–Ni/C) nanoparticles were synthesized by microwave-irradiation using $NaBH_4$ as a reducing agent. Palladium chloride ($PdCl_2$), nickel chloride hexahydrate ($NiCl_2{\cdot}6H_2O$) and sodium borohydride ($NaBH_4$) were purchased from Aldrich. Vulcan XC-72R carbon black was obtained from Cabot Corp., USA with a specific surface area (BET) of 240 $m^2\,g^{-1}$ and an average particle size of 40 nm. Nafion (perfluorosulphonic acid-PTFE copolymer, 5 wt.% mixture of aliphatic alcohol and water) was from Sigma-Aldrich, Germany. Sulfuric acid (H_2SO_4) and methanol (CH_3OH) were from Merck. Double distilled water was used for preparation of solutions and washing.

2.2. Synthesis of electrocatalysts

All prepared electrocatalysts contain total metal loading of 30 wt%. An appropriate amount of Vulcan XC-72R carbon black was ultrasonically mixed with double distilled water for 30 min until a homogeneous suspension was formed. The metal precursors ($PdCl_2$ and $NiCl_2{\cdot}6H_2O$) were then added in an atomic ratio of 1:1 with mechanical stirring for 30 min, followed by sonication for another 30 min. A freshly prepared $NaBH_4$ solution, in which the molar ratio of the metal to $NaBH_4$ was 1:70, was added dropwisely to the mixture with vigorous stirring for 30 min. Heating in a household microwave oven (Caira CA-MW 1025, touch pad digital control, 50 MHz, 1400 W) was operated for 5 min using the pulse mode (20 s on/10 s off). The resulting powder was finally collected by filtration and washed for several times with double distilled water and dried at 80 °C in an air oven for 6 h. For comparison, Pd and Ni electrocatalysts supported on Vulcan XC-72R carbon black were also prepared in the same procedure.

2.3. Physical characterization of electrocatalysts

The phase structure of the prepared electrocatalysts was determined by XRD study that was carried out with the help of Rigaku-D/MAX-PC 2500 X-ray diffractometer equipped with Ni filtered Cu $K\alpha$ as the radiation source. The tube current was 40 mA with a voltage of 40 kV. In order to investigate the size, morphology and dispersion of the electrocatalyst particles, TEM analysis was performed. JEOL-JEM 2010 transmission electron microscope was operated at an accelerating voltage of 160 kV. The catalyst was ultrasonically dispersed in double distilled water to obtain a uniform ink. It was then mounted onto copper grids covered with a carbon film and left to dry in air. EDX analysis was applied to investigate the chemical composition. A scanning electron microscope (JEOL JAX-840) and a POEMS ICP-OES instrument (Thermo Jarrell-Ash Corporation, Franklin, MA, USA) were used.

2.4. Electrochemical characterization of electrocatalysts

Electrochemical studies were carried out using Voltalab 6 potentiostat. A standard three-electrodes cell was constructed to evaluate the electrochemical reactivity of electrocatalysts by cyclic voltammetry and chronoamperometry techniques. A platinum wire was used as the counter electrode, while mercury/mercury oxide Hg/HgO/1.0 M NaOH (MMO) was the reference electrode. The working electrode was a commercial carbon disk covered with a thin layer of Nafion-impregnated catalyst. The potential values mentioned in this work are referred to (MMO) [its potential = +140 mV (NHE)]. Before applying the catalyst powder on the working electrode, carbon surface was polished with emery papers in different grades and cleaned with ethanol. It was then scanned in 0.5 M H_2SO_4 solution in the potential range from −800 to +1600 mV versus mercury/mercurous sulphate electrode [Hg/Hg_2SO_4/1.0 M H_2SO_4 (MMS)] for 50 cycles at a scan rate of 50 mV s^{-1} in order to get an active surface. The thin-film electrode was prepared as follows: 1.1 mg of catalyst powder was dispersed in 0.6 ml 5 wt% Nafion solution and isopropyl alcohol. This ink was then applied onto the working electrode surface using a micropipette. It was left to dry overnight. Cyclic voltammetric experiments were performed in the potential range from −700 to +1300 mV (MMO) in 0.5 M KOH solution in absence and in presence of methanol at a scan rate of 10 mV s^{-1}. All electrochemical measurements were operated in aerated electrolytes at room temperature of 30 °C ± 0.2.

3. Results and discussion

Fig. 1 shows X-ray diffraction patterns of Ni/C, Pd/C and Pd–Ni/C electrocatalysts. The broad peak at 2θ value of about 25° in all patterns is related to the graphite (0 0 2) facet of Vulcan XC-72R carbon black. Another three diffraction peaks are found in X-ray diffraction pattern of Ni/C electrocatalyst to reflect the formation of metallic nickel and nickel hydroxide. According to JCPD (Joint Committee on Powder Diffraction), the reflection at 2θ value of 46.89° corresponds to Ni(1 1 1) plane. On the other hand, (1 0 0) and (1 1 0) facets of $Ni(OH)_2$ appear at 2θ values of 34.05° and 60.45°, respectively [38–40]. For Pd/C electrocatalyst, three diffraction peaks appear at 2θ values of 38.97°, 45.27° and 66.29° as (1 1 1), (2 0 0) and (2 2 0) planes, respectively of face-centered cubic (fcc) crystalline structure of Pd [4,41–43]. For Pd–Ni/C electrocatalyst, the three diffraction planes of Pd are observed at 2θ values of 39.58° (1 1 1),

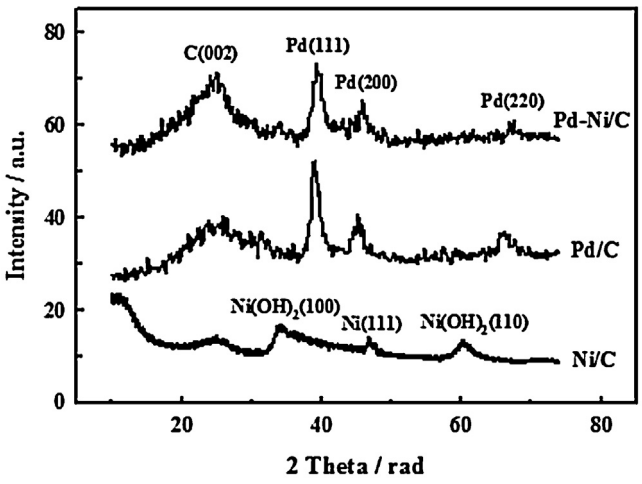

Fig. 1. XRD patterns of Ni/C, Pd/C and Pd–Ni/C electrocatalysts.

Table 1
2θ and d values of different peaks in X-ray diffraction patterns of Ni/C, Pd/C and Pd–Ni/C electrocatalysts.

Ni/C		Pd/C		Pd-Ni/C	
2θ (rad)	d (Å)	2θ (rad)	d (Å)	2θ (rad)	d (Å)
25.010	3.5605	26.230	3.4356	25.560	3.4789
34.049	2.6332	38.970	2.3092	39.580	2.2859
46.890	1.9377	45.270	2.0014	46.000	1.9715
60.447	1.5315	66.290	1.4088	67.310	1.3951

46.00° (2 0 0) and 67.31° (2 2 0). They show positive shift when compared to those of Pd/C electrocatalyst. Many reports have observed this trend at Pd–Ni electrocatalysts [4,5,41,44]. It indicates that nickel atoms were partially entered into Pd lattice with PdNi alloy formation. This opinion is supported by the decreased lattice distance of different Pd diffraction planes in Pd–Ni/C electrocatalyst when compared to those in Pd/C (see Table 1). This corresponds to a lattice contraction with a smaller Pd particle size and a slight decrease in the intensity of diffraction peaks. The average crystallite size of Pd/C and Pd–Ni/C electrocatalysts was calculated based on the broadening of Pd(220) diffraction peak using Debye-Scherrer's equation [45]. It was found as 5.9 and 3 nm for Pd/C and Pd–Ni/C electrocatalysts, respectively. Qi et al. [23] have prepared nanocrystalline $Pd_{40}Ni_{60}$ alloy with Pd crystallite size of 2 nm. Solution phase-based nanocapsule method has been applied to prepare Pd_xNi_y/C catalysts with average Pd particle size of 2.5–3 nm [41]. Core/shell Ni@Pd nanoparticles supported on MWCNTs, prepared by a two-step strategy: impregnation-reduction method and replacement method, had Pd particle size of 3.4 nm [44]. Although nickel could be generally oxidized in air, no diffraction peaks of metallic Ni, Ni oxides or hydroxides are observed in XRD pattern of Pd–Ni/C electrocatalyst. It suggests that nickel may be amorphous in nature or crystalline only in very small region [46,47].

The morphology and particle size of Pd/C, Ni/C and Pd–Ni/C electrocatalysts were investigated by applying transmission electron microscopy in Fig. 2. Spherical particles of carbon black with a mean diameter of 35 nm are clearly observed in TEM images of Pd/C (see Fig. 2a) and Ni/C (see Fig. 2b). Black Pd and Ni particles are highly agglomerated in many areas on carbon support. However, the situation may be reversed in TEM image of Pd–Ni/C (see Fig. 2c). Metal nanoparticles are uniformly distributed on carbon surface without obvious aggregation. Wang et al. have also observed homogeneous dispersion of Pd–Ag and Pd–Pb nanoparticles in Pd–Ag(1:1)/C [48] and Pd–Pb(8:1)/C [49] electrocatalysts, respectively on carbon black support. Particle size of Pd/C, Ni/C and Pd–Ni/C powders was estimated as 6, 6 and 4 nm, respectively. Therefore, the alloy formation between Pd and Ni tends to reduce the size of resulting metal nanoparticles. Li et al. [50] have also reported that the addition of Ni to Pd led to a decrease in the particle size of Pd_xNi_y electrocatalysts. Energy dispersive X-ray analysis of Pd–Ni/C powder is represented in Fig. 3. It is composed of its three components: Pd, Ni and C.

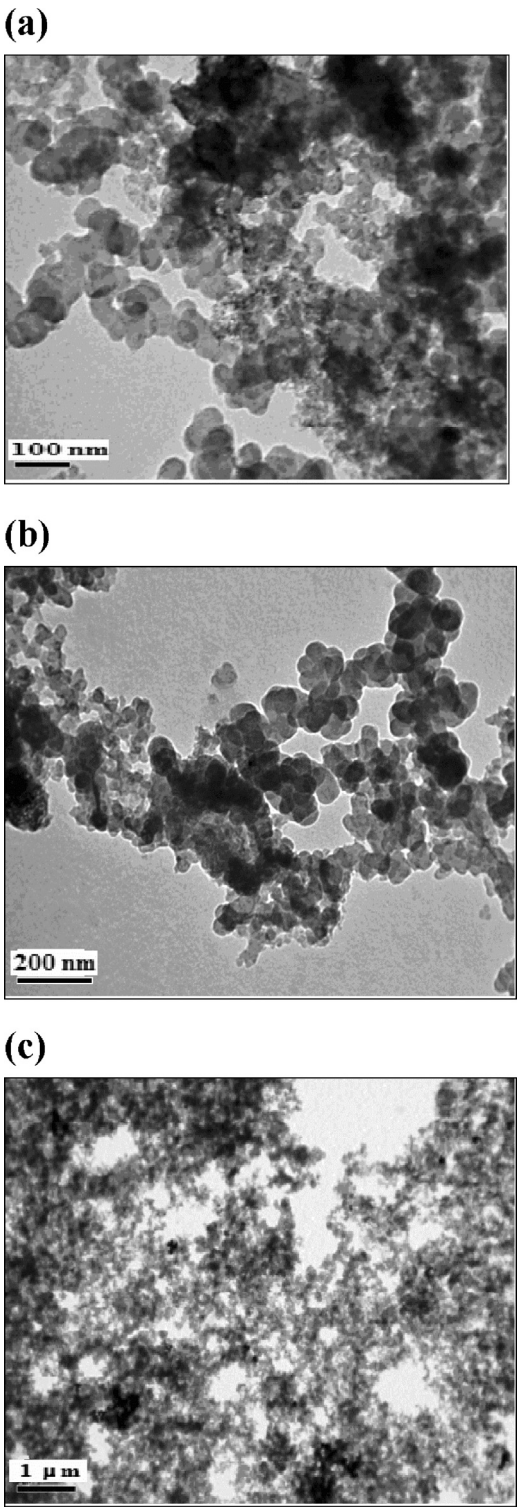

Fig. 2. TEM images of (a) Pd/C, (b) Ni/C and (c) Pd–Ni/C electrocatalysts.

Fig. 4 represents the cyclic voltammograms of Ni/C and Pd–Ni/C electrocatalysts in 0.5 M KOH solution at 10 mV s^{-1}. For Ni/C, nickel

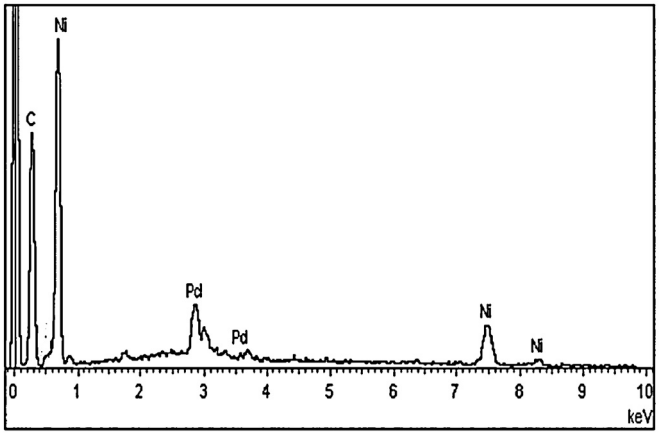

Fig. 3. EDX spectrum of Pd–Ni/C electrocatalyst.

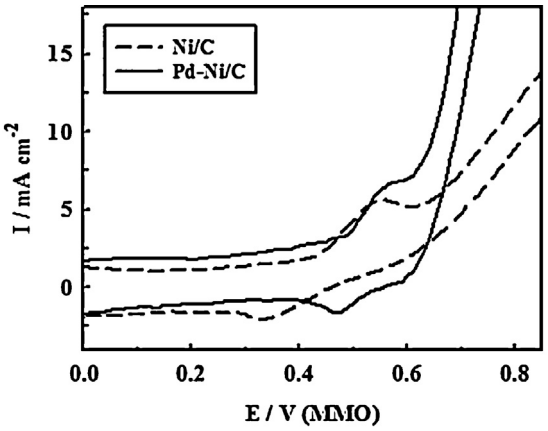

Fig. 4. Cyclic voltammograms of Ni/C and Pd–Ni/C electrocatalysts in 0.5 M KOH solution at 10 mV s^{-1}.

is electrochemically passivated by $Ni(OH)_2$ species in the potential region from −300 up to +425 mV [51,52]. On going towards more positive potential values, an anodic peak appears at +550 mV, where $Ni(OH)_2$ is oxidized to NiOOH according to the following reaction [53,54]:

$$Ni(OH)_2 + OH^- \leftrightarrow NiOOH + H_2O + e^- \quad (1)$$

Oxygen starts to evolve at a potential value of +630 mV. Here, the current of Ni(II) oxidation passes into the current of OH^- oxidation, which is the source of oxygen in alkaline solution by the following reaction [55,56]:

$$4\,OH^- \leftrightarrow O_2 + 2H_2O + 4e^- \quad (2)$$

NiOOH is reduced in the backward direction at a potential value of +340 mV. When Pd was added in Pd–Ni/C electrocatalyst, $Ni(OH)_2$/NiOOH redox couple was observed at +580 and +470 mV in the forward and backward directions, respectively. Although this redox couple is shifted towards more positive potential values when compared to that at Ni/C electrocatalyst, the peak potential separation (ΔE) at Pd–Ni/C is lower (110 mV). The current

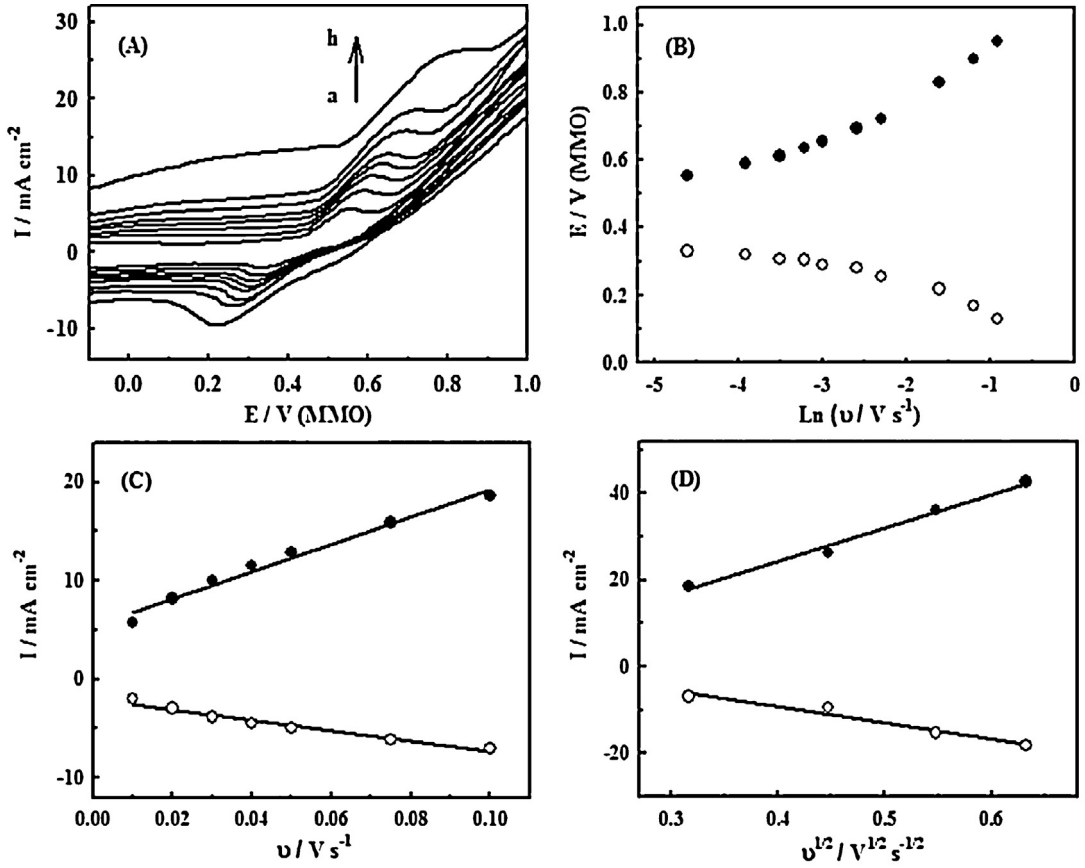

Fig. 5. (A) Cyclic voltammograms of Ni/C electrocatalyst in 0.5 M KOH solution at scan rates of (a) 10, (b) 20, (c) 30, (d) 40, (e) 50, (f) 75, (g) 100 and (h) 200 mV s^{-1}. (B) The dependence of the anodic and cathodic peak potential values on the natural logarithm of the scan rate. The linear dependence of the anodic and cathodic peak current density on the scan rate at lower values (10–100 mV s^{-1}) (C) and on the square root of the scan rate at higher values (100–400 mV s^{-1}) (D).

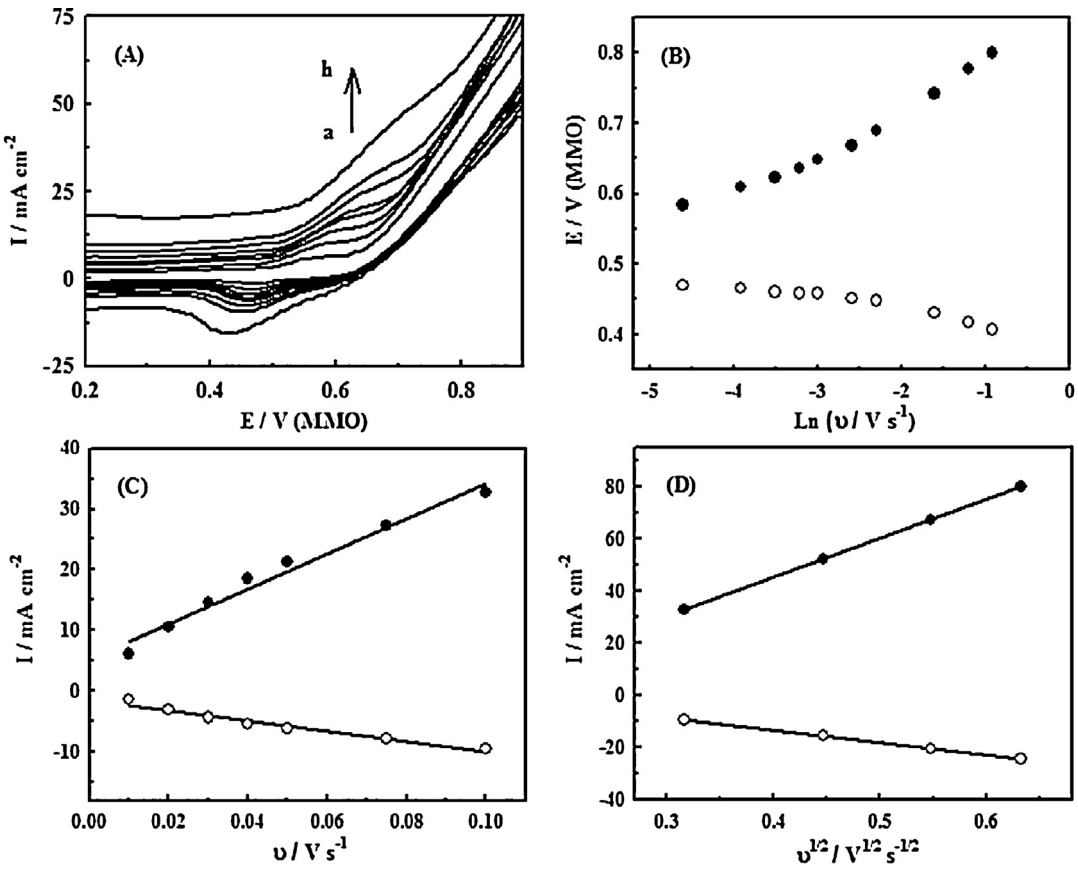

Fig. 6. (A) Cyclic voltammograms of Pd–Ni/C electrocatalyst in 0.5 M KOH solution at scan rates of (a) 10, (b) 20, (c) 30, (d) 40, (e) 50, (f) 75, (g) 100 and (h) 200 mV s^{-1}. (B) The dependence of the anodic and cathodic peak potential values on the natural logarithm of the scan rate. The linear dependence of the anodic and cathodic peak current density on the scan rate at lower values (10–100 mV s^{-1}) (C) and on the square root of the scan rate at higher values (100–400 mV s^{-1}) (D).

density value of the anodic side of $Ni(OH)_2$/NiOOH transformation at Pd–Ni/C electrocatalyst is also higher by 1.16 times than that at Ni/C. This is an indication of subjecting an increased number of nickel active sites to oxidation at Pd–Ni/C electrode surface. Oxygen evolution is observed at a lower potential value (+610 mV) with a rapid current density increase due to the formation of surface oxides of Pd–Ni catalyst [26].

The electrochemical behaviour of Ni/C and Pd–Ni/C electrocatalysts in 0.5 M KOH solution was investigated at different scan rates in Figs. 5 and 6, respectively. In general, an increase in the current density of $Ni(OH)_2$/NiOOH redox couple is shown with increasing the scan rate. Moreover, the anodic peak potential is shifted in the positive direction, while the cathodic one is shifted towards more negative potential values. Laviron [57] presented a theory for manifesting the slow electron transfer of attached electroactive species. The electron transfer coefficient (α) and electron transfer rate constant (k_s) can be calculated based on Laviron's theory:

$$E_{pa} = E_o + \frac{RT}{\{(1-\alpha)nF\}} \times \ln\left\{\frac{(1-\alpha)nF\upsilon}{RTk_s}\right\} \quad (3)$$

$$E_{pc} = E_o + \frac{RT}{(\alpha nF)} \times \ln\left(\frac{\alpha nF\upsilon}{RTk_s}\right) \quad (4)$$

$$\ln k_s = \alpha\ \ln(1-\alpha) + (1-\alpha)\ln\alpha - \ln\left(\frac{RT}{nF\upsilon}\right) - \frac{\alpha(1-\alpha)nF\Delta E}{RT} \quad (5)$$

where: E_{pa} and E_{pc} are the anodic and cathodic peak potentials in V, respectively, E_o is the standard electrode potential, R is the universal gas constant (8.314 J mol^{-1} K^{-1}), T is the absolute temperature in K, F is Faraday's constant (96485.3 C mol^{-1}), n is the electron transfer number, υ is the scan rate in V s^{-1} and k_s is the electron transfer rate constant in s^{-1}. The anodic and cathodic peak potentials are plotted versus the natural logarithm of scan rate at Ni/C and Pd–Ni/C electrocatalysts in Figs. 5B and 6B, respectively. From the slope of the linear portions at higher scan rates (100–400 mV s^{-1}) and using Eqs. (3) and (4), the electron transfer coefficient value (α) was calculated as 0.522 and 0.700 at Ni/C and Pd–Ni/C electrocatalysts, respectively. From this α value and using Eq. (5), the electron transfer rate constant (k_s) was estimated as 2.688×10^{-3} and 0.312 s^{-1} at Ni/C and Pd–Ni/C electrocatalysts, respectively. The larger α value at Pd–Ni/C indicates its higher ability to promote electrons between the catalyst nanoparticles and the electrode surface.

The current density values of anodic and cathodic peaks of $Ni(OH)_2$/NiOOH redox couple at Ni/C and Pd–Ni/C electrocatalysts are linearly dependent on the scan rate at low values from 10 to 100 mV s^{-1} in Figs. 5C and 6C, respectively. This may be due to the electrochemical activity of immobilized redox species at the surface of modified electrodes. From the slope of this relation and using the following equation, the electrode surface coverage (Γ^*) can be calculated [58]:

$$I_p = \left(\frac{n^2F^2}{4RT}\right)\upsilon A\Gamma^* \quad (6)$$

where I_p is the peak current in Ampere, A is the electrode surface area in cm^2 and Γ^* is the surface coverage of redox species in mol cm^{-2}. By taking the average of both anodic and cathodic sides, Γ^* was calculated as 1.020×10^{-7} and 1.998×10^{-7} mol cm^{-2} at Ni/C and Pd–Ni/C electrocatalysts, respectively. At scan rates higher than 100 mV s^{-1}, the current density values of $Ni(OH)_2$/NiOOH

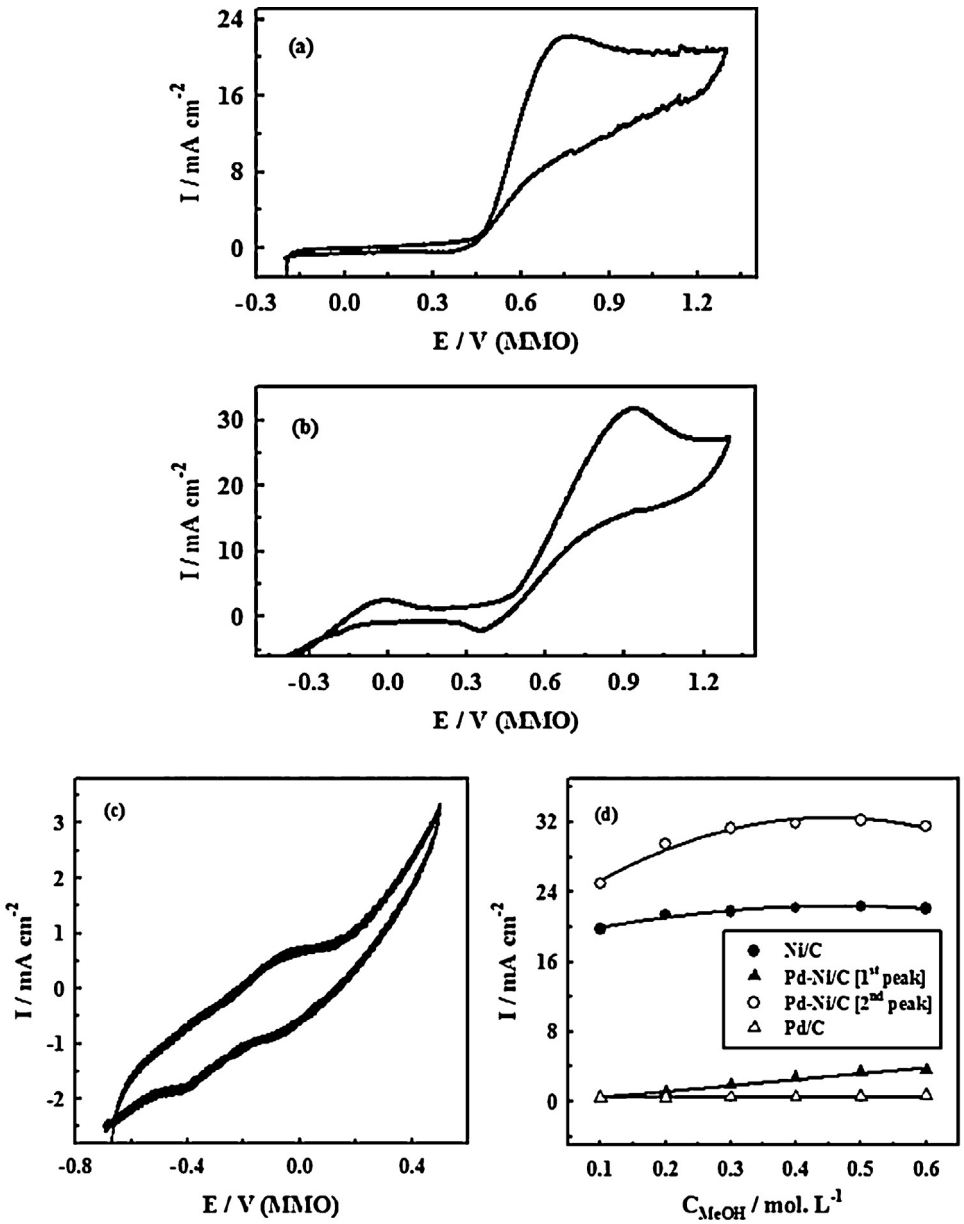

Fig. 7. Cyclic voltammograms of methanol oxidation at (a) Ni/C, (b) Pd–Ni/C and (c) Pd/C electrocatalysts in (0.6 M MeOH + 0.5 M KOH) solution at 10 mV s^{-1}. (d) Variation of methanol oxidation peak current density values with its concentration at Ni/C, Pd/C and Pd–Ni/C electrocatalysts.

redox couple are proportional to the square root of the scan rate as evident in Figs. 5D and 6D at Ni/C and Pd–Ni/C electrocatalysts, respectively. It signifies the dominance of a diffusion-controlled process as the rate-limiting step in the redox transition of the modified electrode. This was reported for many nickel modified electrodes [53,59–62].

The electrocatalysts were then introduced into another cell containing 0.6 M methanol in 0.5 M KOH solution and cyclic voltammograms were recorded at 10 mV s^{-1} (see Fig. 7a and b for Ni/C and Pd–Ni/C electrocatalysts, respectively). For Ni/C electrocatalyst, methanol oxidation peak is shown at a potential value of +735 mV with a current density of 22.13 mA cm^{-2}. Methanol oxidation reaction coincides with $Ni(OH)_2$/NiOOH transformation. This observation supports the dependence of the oxidation process on NiOOH formation [54,63,64]. The current density of nickel oxyhydroxide reduction peak in the backward direction is also greatly reduced with a potential shift in the positive direction by 74 mV when compared to the corresponding one in 0.5 M KOH solution. This is a result of the partial consumption of NiOOH species during methanol oxidation reaction to regenerate $Ni(OH)_2$ in accordance with the following equation [65,66]:

$$\text{NiOOH} + \text{methanol} \rightarrow \text{Ni(OH)}_2 + \text{products} \quad (7)$$

For Pd–Ni/C electrocatalyst, two methanol oxidation peaks appear at potential values of 0 and +913 mV. The first oxidation peak (at 0 mV) is absent in the cyclic voltammogram of methanol oxidation at Ni/C electrocatalyst in Fig. 7a. In addition, when Pd/C electrocatalyst was scanned in (0.6 M MeOH + 0.5 M KOH) solution at 10 mV s^{-1}, an oxidation peak was shown at 0 mV (see Fig. 7c). It corresponds to the oxidation of freshly chemisorbed methanol species at Pd surface [4,8,25,67,68]. For the first sight, we may think that only Pd is responsible for methanol oxidation at 0 mV. However, the current density of this oxidation peak at Pd–Ni/C electrocatalyst may defeat this opinion. It shows 3.84 folds increment when compared to that at Pd/C. Jin et al. [69] did not also have an oxidation peak for allyl alcohol at Ni/C in this potential region.

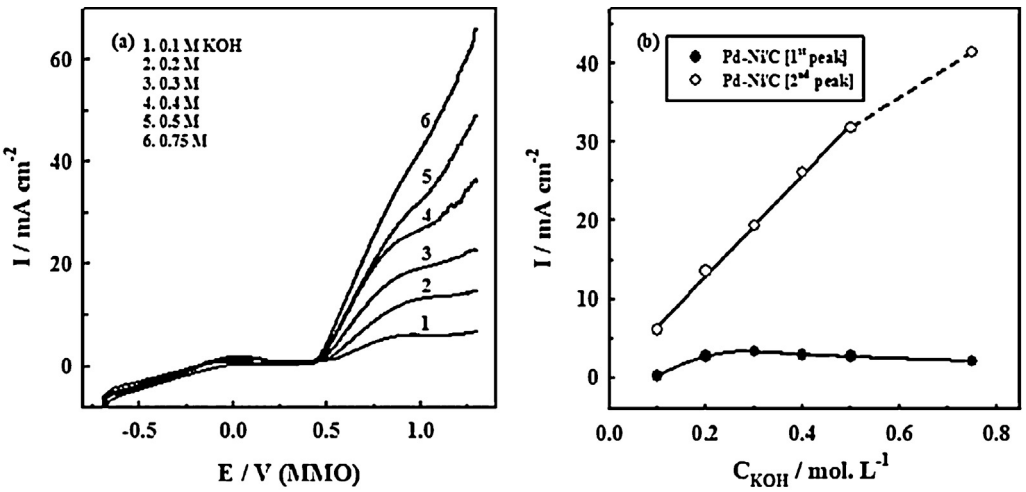

Fig. 8. (a) Linear sweep voltammograms of methanol oxidation at Pd–Ni/C electrocatalyst in 0.6 M methanol in KOH solution with different concentrations at 10 mV s^{-1}. (b) Variation of methanol oxidation peak current density values with KOH concentration at Pd–Ni/C electrocatalyst.

However, they observed an enhanced oxidation peak at Pd_xNi_y/C electrocatalysts in relation to that at Pd/C. They suggested that the activity of Pd is improved by adding Ni in Pd_xNi_y/C electrocatalysts. Many workers have also supported this result [4,5,25]. That is to say, in the oxidation of methanol at Pd–Ni/C electrocatalyst at 0 mV, Pd acts as the main active sites, while Ni helps in the catalytic function to finally have a catalytic activity dependent on both Pd and Ni. Zhao et al. [5] have examined the electrocatalytic activity of Ni@Pd/MWCNTs electrocatalyst for methanol oxidation in (1 M methanol + 0.5 M NaOH) solution at a scan rate of 50 mV s^{-1}. The onset potential of methanol oxidation peak was observed at −540 and −430 mV (MMO) at Ni@Pd/MWCNTs and Pd/MWCNTs electrocatalysts, respectively. On the other hand, Ni@Pd/MWCNTs showed an oxidation mass specific peak current of 770.7 mA mg^{-1} Pd compared to 315.1 mA mg^{-1} Pd at Pd/MWCNTs. The second methanol oxidation peak [at +913 mV] at Pd–Ni/C electrocatalyst shows higher current density by 1.43 times than that at Ni/C. All work concerning alcohol oxidation at Pd–Ni based electrocatalysts dealt with the first potential region [at 0 mV]. However, Kumar et al. [26] have studied methanol oxidation at electrodeposited Pd–Ni alloy in an extended potential range. They recorded an ill-defined oxidation peak at about 700 mV (MMO) with two folds increment in its current density when compared to that at plain nickel electrode. Pd–Ni alloy containing 4.5 at% Pd showed an onset potential value of methanol oxidation at 438 mV (MMO) in (1 M methanol + 1 M KOH) solution at 20 mV s^{-1} with a current density of 45 mA cm^{-2}. The onset potential of methanol oxidation at Pd - Ni alloy coincides with OH^- adsorption. More predominant cathodic peak is observed at Pd–Ni/C electrocatalyst with a lowered current density value by 2.8 times in relation to that in 0.5 M KOH solution. The variation of methanol oxidation peak current density values with methanol concentration at Pd/C, Ni/C and Pd–Ni/C electrocatalysts is represented in Fig. 7d. As methanol concentration increases, methanol oxidation current density values increase at the two oxidation positions at Pd–Ni/C electrocatalyst. Higher oxidation current density values are noticed at Pd–Ni/C electrocatalyst when compared to those at Pd/C and Ni/C.

The effect of varying KOH concentration on methanol oxidation reaction at Pd–Ni/C electrocatalyst was studied in Fig. 8. Linear sweep voltammograms were recorded in 0.6 M methanol in KOH solution with different concentrations at 10 mV s^{-1} in Fig. 8a. The current density of the first methanol oxidation peak slightly increases with KOH concentration up to 0.3 M value. Afterwards, no appreciable change was shown. On the other hand, linear dependence of the current density of the second oxidation peak on KOH concentration was observed till it deviates starting from 0.5 M value. Fig. 8b describes the variation of methanol oxidation peak current density values with KOH concentration at Pd–Ni/C electrocatalyst. According to this result, 0.5 M KOH solution is chosen in the present work to study the electrocatalytic performance of Pd–Ni/C towards methanol oxidation reaction.

Linear sweep voltammograms of methanol oxidation at Ni/C and Pd–Ni/C electrocatalysts in (0.6 M MeOH + 0.5 M KOH) solution at different scan rates are represented in Fig. 9a and b, respectively. The oxidation peak current density at both electrocatalysts increases with increasing the scan rate. The second oxidation peak at Pd–Ni/C electrocatalyst has higher current density values when compared to that at Ni/C. A plot of methanol oxidation peak current density at both electrocatalysts versus the square root of the scan rate shows a linear relationship (see Fig. 9c). It suggests that the electrocatalytic oxidation of methanol at Ni/C and Pd–Ni/C electrocatalysts may be controlled by a diffusion process [70,71]. Moreover, as the scan rate increases, the oxidation peak potential is shifted towards more positive values. This potential shift is possibly due to the IR drop generated at high current density values [72]. Higher oxidation potential values are observed at Pd–Ni/C electrocatalyst relative to those at Ni/C. A linear plot was obtained between the natural logarithm of scan rate and oxidation peak potential at both electrocatalysts (see Fig. 9d). It indicates that the oxidation of methanol is an irreversible electrode process [73].

Chronoamperometry could be used to evaluate the catalytic rate constant for the reaction between methanol and the prepared electrocatalysts. Fig. 10a, a' and b, b' shows double-step chronoamperograms of Ni/C and Pd–Ni/C electrocatalysts, respectively in absence and in presence of methanol over a concentration range of 0.05–0.6 M. The applied potential steps were 750 and 430 mV (MMO), respectively. It is observed that as methanol concentration increases, the oxidation current density at Pd–Ni/C electrocatalyst increases at the first potential step up to 0.6 M methanol. However, this trend is observed at Ni/C electrocatalyst only up to 0.3 M methanol. No current density change was recorded at higher methanol concentrations. The catalytic rate constant k can be calculated according to the following equation [58]:

$$I_C/I_L = [\gamma^{0.5}(\pi^{0.5}\,\mathrm{erf}(\gamma^{0.5})) + \exp(-\gamma/\gamma^{0.5})] \quad (8)$$

where I_C and I_L are the current density values of the electrocatalyst in the presence and in absence of methanol, respectively and $\gamma = kC_0t$ is the argument of the error function. The catalytic rate

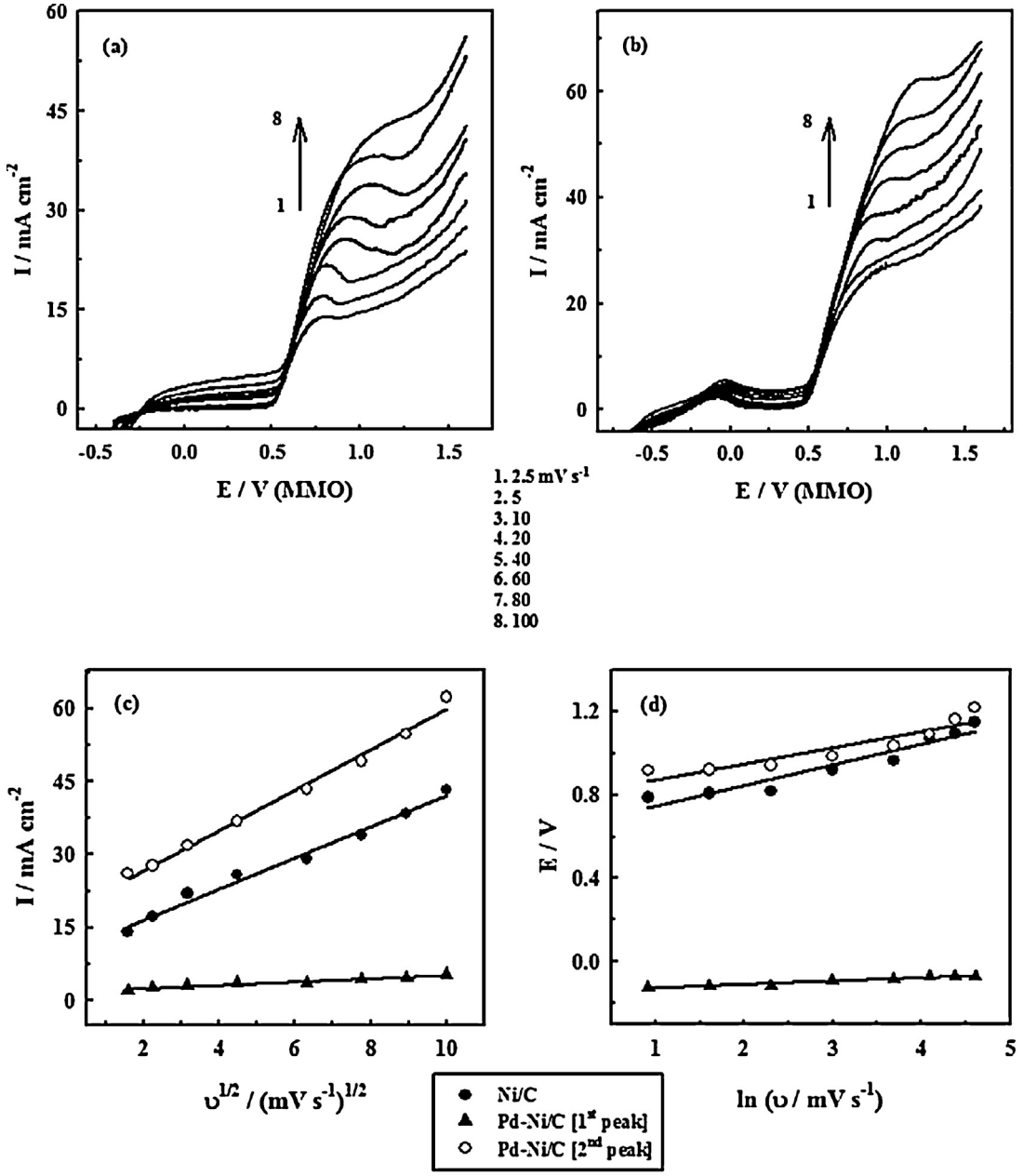

Fig. 9. Linear sweep voltammograms of (a) Ni/C and (b) Pd–Ni/C electrocatalysts in (0.6 M MeOH + 0.5 M KOH) solution at different scan rates. Their oxidation peak current density values are plotted as a function of the square root of scan rate in (c). A plot of methanol oxidation peak potential values at Ni/C and Pd–Ni/C electrocatalysts versus the natural logarithm of scan rate is shown in (d).

constant is k in $cm^3\,mol^{-1}\,s^{-1}$, C_0 is the bulk concentration of methanol in $mol\,cm^{-3}$, erf is the error function and t is the elapsed time in s. In such cases where $\gamma > 1.5$, erf $(\gamma^{0.5})$ is almost equal to unity and the above equation can be reduced to the following law:

$$I_C/I_L = \gamma^{0.5}\,\pi^{0.5} = \pi^{0.5}\,(kC_0t)^{0.5} \quad (9)$$

Plotting the current ratio (I_C/I_L) with respect to the square root of time shows a linear relationship at Ni/C electrocatalyst using different concentrations of methanol in Fig. 10c. When the corresponding relation for Pd–Ni/C electrocatalyst is compared in 0.2 M methanol concentration (see Fig. 10d), higher I_C/I_L values are observed. Based on the slope of this line, the catalytic rate constant of methanol oxidation reaction at Ni/C and Pd–Ni/C electrocatalysts was found to be 1.80×10^3 and $5.88 \times 10^3\,cm^3\,mol^{-1}\,s^{-1}$, respectively. This k value of methanol oxidation at Pd–Ni/C, prepared by microwave irradiation, is higher than that for methanol oxidation at nickel-poly(*o*-aminophenol)-modified carbon paste electrode ($86.70\,cm^3\,mol^{-1}\,s^{-1}$) [74], electrochemically deposited $Ni(OH)_2$ layer at Ni–Cu alloy ($1.98 \times 10^3\,cm^3\,mol^{-1}\,s^{-1}$) [75] and poly Ni(II) curcumin modified glassy carbon electrode ($2.04 \times 10^3\,cm^3\,mol^{-1}\,s^{-1}$) [76].

When the net current of methanol oxidation reaction at Pd–Ni/C electrocatalyst in various methanol concentrations (0–0.6 M) is plotted against the minus square root of time, straight lines are obtained (see Fig. 10e). Therefore, it confirms that the oxidation reaction is a diffusion-controlled process. The transient current density value at Pd–Ni/C electrocatalyst in (0.2 M MeOH + 0.5 M

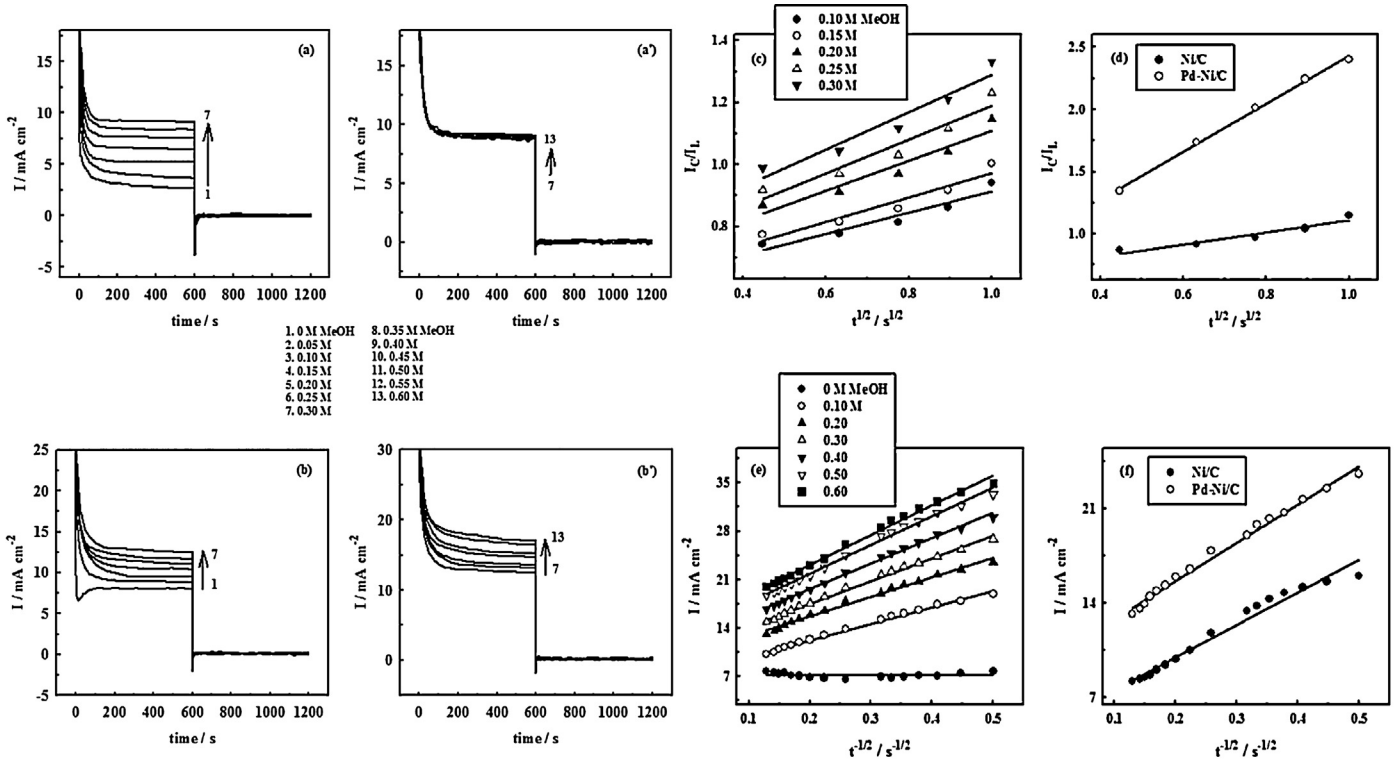

Fig. 10. Chronoamperograms of Ni/C (a, a') and Pd-Ni/C (b, b') electrocatalysts in 0.5 M KOH solution with various concentrations of methanol (0, 0.05, 0.10, 0.15, 0.20, 0.25, 0.30, 0.35, 0.40, 0.45, 0.50, 0.55 and 0.60 M). The potential steps were 750 and 430 mV (MMO), respectively. (c) Dependency of (I_C/I_L) on $t^{1/2}$ derived from the data of chronoamperograms in (a) at Ni/C electrocatalyst. (d) Comparison between I_C/I_L values in (0.2 M MeOH + 0.5 M KOH) solution with respect to $t^{1/2}$ at Ni/C and Pd–Ni/C electrocatalysts. (e) Dependency of transient current density on $t^{-1/2}$ at Pd–Ni/C electrocatalyst in 0.5 M KOH solution containing various methanol concentrations. (f) Comparison between the transient current density values in (0.2 M MeOH + 0.5 M KOH) solution with respect to $t^{-1/2}$ at Ni/C and Pd–Ni/C electrocatalysts.

KOH) solution is higher than that at Ni/C as shown in Fig. 10f. The diffusion coefficient of methanol was calculated according to Cottrell's equation [77]:

$$I = nFAD^{0.5}C\pi^{-0.5}t^{-0.5} \quad (10)$$

where I is the net current in Ampere, D is the diffusion coefficient in $cm^2\,s^{-1}$ and C is the bulk concentration of methanol in $mol\,cm^{-3}$. The value of the diffusion coefficient of methanol was calculated as 2.64×10^{-6} and $7.78 \times 10^{-6}\,cm^2\,s^{-1}$ at Ni/C and Pd–Ni/C electrocatalysts, respectively. This D value at Pd–Ni/C is higher than that at nickel-copper alloy modified glassy carbon electrode ($2.00 \times 10^{-6}\,cm^2\,s^{-1}$) [53] and nickel-manganese alloy modified graphite electrode ($4.00 \times 10^{-6}\,cm^2\,s^{-1}$) [62].

The long-term stability of the electrocatalyst is an important parameter. This could be examined by applying cyclic voltammetry and chronoamperometry techniques. The first and tenth cycles of Ni/C, Pd–Ni/C and Pd/C electrocatalysts in (0.6 M MeOH + 0.5 M KOH) solution are shown in Fig. 11a–c, respectively at a scan rate of $10\,mV\,s^{-1}$. The anodic peak current density gradually decreases with potential cyclization. After 10 cycles, the current density decay at Ni/C and the second oxidation peak at Pd–Ni/C electrocatalyst reached 66.94% and 98.56%, respectively with respect to its initial value in the first cycle. This catalytic activity loss with repeated potential scanning may result from the consumption of methanol during consecutive cyclic voltammograms. The change in the nickel structure due to the perturbation of the potentials in aqueous solution could result in the formation of poisoning species, especially in the presence of organic compound such as methanol. The diffusion process between the electrode surface and the bulk solution could play an additional role. With increasing the scan number, methanol gradually diffuses from the bulk solution to the electrode surface causing a decrease in its concentration. For Pd/C electrocatalyst, the oxidation current density in 10th cycle decreases to get 71% of that of 1st cycle (see Fig. 11c). However, the first oxidation peak at Pd–Ni/C electrocatalyst increases with potential cyclization to get 149% of that of the first cycle after 10 cycles. The poor durability of Pd/C is attributed to ease aggregation of Pd nanoparticles, their dissolution from the carbon support into the electrolyte or poisoning by the intermediates [78,79]. Wang et al. [80] have evaluated the long-term durability of Pd/C and Pd/graphene electrocatalysts during formic acid oxidation by continuous potential scanning to follow the changes in the anodic peak current density with cycle number. It was found that the peak current density of Pd/C electrocatalyst sharply decreases to get 19% of its initial value after 50 cycles. TEM images showed severe agglomeration with particle size increase of Pd on conventional carbon after the durability test. In contrast, the peak current density of Pd/graphene initially increases and then levels off with no obvious degradation even for 200 cycles. The stability trend of Pd/C, Ni/C and Pd–Ni/C electrocatalysts was also studied by chronoamperometry in Fig. 11d. These chronoamperograms were recorded at a potential value of 0 mV at Pd/C and the first oxidation peak of Pd–Ni/C and 750 mV at Ni/C and the second oxidation peak of Pd - Ni/C electrocatalysts for 80 min in (0.6 M MeOH + 0.5 M KOH) solution. It is found that methanol oxidation current density on all electrocatalysts rapidly decreases at first until the steady state value is attained. This decay is attributed to the formation of some Pd (and/or Ni) oxides/hydroxides and adsorbed intermediates in methanol oxidation reaction. After 80 min, the limiting current density values at Pd–Ni/C electrocatalyst (the first and second oxidation peaks) are 1.11 and $14.05\,mA\,cm^{-2}$, respectively. They record an increase by 4 and 1.67 times when compared to that at Pd/C and Ni/C, respectively. This result confirms that Pd–Ni/C electrocatalyst is more efficient and poisoning tolerant.

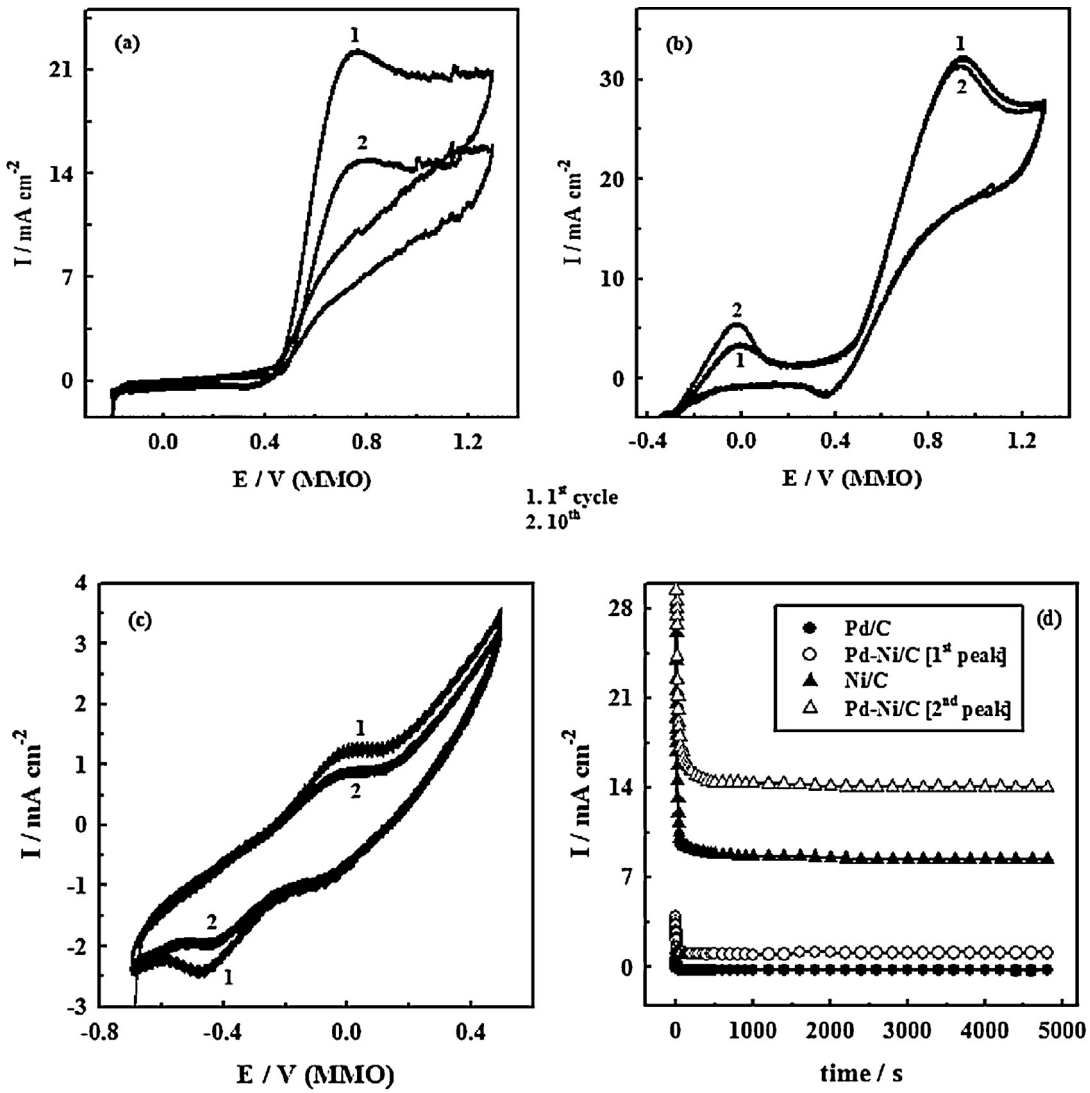

Fig. 11. The 1st and 10th cycles of methanol oxidation at (a) Ni/C, (b) Pd–Ni/C and (c) Pd/C electrocatalysts in (0.6 M MeOH + 0.5 M KOH) solution at 10 mV s^{-1}. (d) Chronoamperograms of these electrocatalysts for 80 min. Two potential values were stepped: 0 mV at Pd/C and the first oxidation peak at Pd–Ni/C and 750 mV at Ni/C and the second oxidation peak at Pd–Ni/C electrocatalyst.

The enhanced electrocatalytic activity at Pd–Ni/C electrocatalyst may be attributed to the modification of the electronic state of Pd as a result of alloy formation between Ni and Pd as shown by XRD study. According to the d-band theory of Nørskov and co-workers [81–83], there is a direct correlation between the reactivity and the d-band center value of noble metal alloyed with Fe or Ni or Co. The thin layer of noble metal would become compressive in atom arrangement when supported on Fe or Ni or Co substrate. They reveal that the narrow down of the d-band weakens CO adsorption because of decreased back-donation from Pd to anti-bonding CO orbitals [84]. In addition, electrons could be transferred from Ni to Pd since Ni is less electronegative [1.91] than Pd [2.20] [25]. This can decrease the Pd–CO binding energy, improve the oxidation of CO-like intermediates from methanol dehydrogenation and enhance the adsorption and oxidation of methanol molecules [85,86]. The bifunctional mechanism could also play an important role in improving the catalytic performance of Pd–Ni/C electrocatalyst. Ni is more oxophilic than Pd and has the capacity to generate surface Ni–OH moieties at a low potential value [38]. This hydroxyl species could oxidize CO_{ads} poisoning intermediates to liberate active Pd sites for further oxidation reaction. Shen et al. [87] reported that the electrocatalytic activity of Pd/C towards methanol oxidation is improved by adding NiO. The decreased particle size of Pd–Ni/C electrocatalyst in comparison to that of Pd/C and Ni/C could also increase the exposed surface area for the oxidation reaction, thus enhancing the catalytic performance.

4. Conclusion

Pd–Ni nanoparticles were uniformly deposited onto Vulcan XC-72R carbon black using microwave-irradiation. An alloy was formed between Ni and Pd in Pd–Ni/C powder as shown in XRD pattern. The electron transfer coefficient (α) increased from 0.522 at Ni/C to 0.700 after adding Pd. The increased electron transfer rate constant (k_s) at Pd–Ni/C electrocatalyst (0.312 s^{-1}) highly promotes electrons between the catalyst nanoparticles and the electrode surface. Methanol was oxidized at two potential values at Pd–Ni/C electrocatalyst: 0 and +913 mV. The current density of the first and second methanol oxidation peaks increased by 3.84 and 1.43 times in relation to those at Pd/C and Ni/C electrocatalysts, respectively. The linear relationship of methanol oxidation current density versus the square root of scan rate at Ni/C and Pd–Ni/C suggests the dominance of diffusion-controlled process. Using double-step chronoamperometry, the catalytic rate constant

of methanol oxidation reaction was calculated as 1.80×10^3 and 5.88×10^3 cm^3 mol^{-1} s^{-1} at Ni/C and Pd–Ni/C, respectively. The long-term stability of Pd–Ni/C is better than that of Ni/C and Pd/C electrocatalysts.

References

[1] C. Rayment, S. Sherwin, Introduction to Fuel Cell Technology, Notre Dame, IN, 2003, pp. 57 (Chapter 8).
[2] R. Wang, H. Wang, B. Wei, W. Wang, Z. Lei, Int. J. Hydrogen Energy 35 (2010) 10081.
[3] J. Liu, J. Ye, C. Xu, S.P. Jiang, Y. Tong, J. Power Sources 177 (2008) 67.
[4] Z. Liu, X. Zhang, L. Hong, Electrochem. Commun. 11 (2009) 925.
[5] Y. Zhao, X. Yang, J. Tian, F. Wang, L. Zhan, Int. J. Hydrogen Energy 35 (2010) 3249.
[6] I. Danaee, M. Jafarian, F. Forouzandeh, F. Gobal, M.G. Mahjani, Int. J. Hydrogen Energy 34 (2009) 859.
[7] R.N. Singh, A. Singh, Anindita, D. Mishra, Int. J. Hydrogen Energy 33 (2008) 6878.
[8] Y.-H. Qin, H.-H. Yang, X.-S. Zhang, P. Li, C.-A. Ma, Int. J. Hydrogen Energy 35 (2010) 7667.
[9] J.B. Xu, T.S. Zhao, S.Y. Shen, Y.S. Li, Int. J. Hydrogen Energy 35 (2010) 6490.
[10] Y. Wang, X. Wang, C.M. Li, Appl. Catal. B 99 (2010) 229.
[11] S.T. Nguyen, H.M. Law, H.T. Nguyen, N. Kristian, S. Wang, S.H. Chan, X. Wang, Appl. Catal. B 91 (2009) 507.
[12] R.N. Singh, A. Singh, Anindita, J. Solid State Electrochem. 13 (2009) 1259.
[13] F.P. Hu, Z. Wang, Y. Li, C. Li, X. Zhang, P.K. Shen, J. Power Sources 177 (2008) 61.
[14] M. Watanabe, S. Motoo, J. Electroanal. Chem. Interfacial Electrochem. 60 (1975) 259.
[15] O. Savadogo, K. Lee, K. Oishi, S. Mitsushima, N. Kamiya, K.-I. Ota, Electrochem. Commun. 6 (2004) 105.
[16] M. Grdeń, M. Łukaszewski, G. Jerkiewicz, A. Czerwiński, Electrochim. Acta 53 (2008) 7583.
[17] Z. Yan, G. He, G. Zhang, H. Meng, P.K. Shen, Int. J. Hydrogen Energy 35 (2010) 3263.
[18] F. Kadirgan, S. Beyhan, T. Atilan, Int. J. Hydrogen Energy 34 (2009) 4312.
[19] Y.N. Wu, S.J. Liao, Y.L. Su, J.H. Zeng, D. Dang, J. Power Sources 195 (2010) 6459.
[20] Y. Tang, Y. Chen, P. Zhou, Y. Zhou, L. Lu, J. Bao, T.J. Lu, Solid State Electrochem. 14 (2010) 2077.
[21] R. Li, H. Hao, W.-B. Cai, T. Huang, A. Yu, Electrochem. Commun. 12 (2010) 901.
[22] J. Wang, G. Yin, Y. Chen, R. Li, X. Sun, Int. J. Hydrogen Energy 34 (2009) 8270.
[23] Z. Qi, H. Geng, X. Wang, C. Zhao, H. Ji, C. Zhang, J. Xu, Z. Zhang, J. Power Sources 196 (2011) 5823.
[24] F. Miao, B. Tao, L. Sun, T. Liu, J. You, L. Wang, P.K. Chu, J. Power Sources 195 (2010) 146.
[25] R.N. Singh, Anindita, A. Singh, Int. J. Hydrogen Energy 34 (2009) 2052.
[26] K.S. Kumar, P. Haridoss, S.K. Seshadri, Surf. Coat. Technol. 202 (2008) 1764.
[27] T.S. Ahmadi, Z.L. Wang, T.C. Green, A. Henglein, M.A. El-Sayed, Science 272 (1996) 1924.
[28] C. Coutanceau, S. Brimaud, C. Lamy, J.-M. Léger, L. Dubau, S. Rousseau, F. Vigier, Electrochim. Acta 53 (2008) 6865.
[29] Z. Liu, E.T. Ada, M. Shamsuzzoha, G.B. Thompson, D.E. Nikles, Chem. Mater. 18 (2006) 4946.
[30] N. Fujiwara, K. Yasuda, T. Ioroi, Z. Siroma, Y. Miyazaki, Electrochim. Acta 47 (2002) 4079.
[31] J. Wang, G. Yin, Y. Shao, Z. Wang, Y. Gao, J. Electrochem. Soc. 154 (2007) B687.
[32] P. Sivakumar, V. Tricoli, Electrochim. Acta 51 (2006) 1235.
[33] C. Bock, C. Paquet, M. Couillard, G.A. Botton, B.R. MacDougall, J. Am. Chem. Soc. 126 (2004) 8028.
[34] B. Rajesh, K.R. Thampi, J.-M. Bonard, N. Xanthopoulos, H.J. Mathieu, B. Viswanathan, J. Phys. Chem. B 107 (2003) 2701.
[35] M.K. Jeon, K.R. Lee, H.J. Jeon, S.I. Woo, J. Appl. Electrochem. 39 (2009) 1503.
[36] C.W.B. Bezerra, L. Zhang, H. Liu, K. Lee, A.L.B. Marques, E.P. Marques, H. Wang, J. Zhang, J. Power Sources 173 (2007) 891.
[37] M. Tsuji, M. Hashimoto, Y. Nishizawa, M. Kubokawa, T. Tsuji, Chem. Eur. J 11 (2005) 440.
[38] S.Y. Shen, T.S. Zhao, J.B. Xu, Y.S. Li, J. Power Sources 195 (2010) 1001.
[39] L. Xiao, J.-T. Lu, P.-F. Liu, L. Zhuang, J. Yan, Y. Hu, B. Mao, C. Lin, J. Phys. Chem. B 109 (2005) 3860.
[40] C.-B. Wang, G.-Y. Gau, S.-J. Gau, C.-W. Tang, J.-L. Bi, Catal. Lett. 101 (2005) 241.
[41] Z. Zhang, L. Xin, K. Sun, W. Li, Int. J. Hydrogen Energy 36 (2011) 12686.
[42] F. Cheng, H. Wang, Z. Sun, M. Ning, Z. Cai, M. Zhang, Electrochem. Commun. 10 (2008) 798.
[43] C. Xu, L. Cheng, P. Shen, Y. Liu, Electrochem. Commun. 9 (2007) 997.
[44] M. Zhang, Z. Yan, J. Xie, Electrochim. Acta 77 (2012) 237.
[45] J.B. Xu, T.S. Zhao, Z.X. Liang, J. Phys. Chem. C 112 (2008) 17362.
[46] M. Simões, S. Baranton, C. Coutanceau, Appl. Catal. B 93 (2010) 354.
[47] S.L. Medway, C.A. Lucas, A. Kowal, R.J. Nichols, D. Johnson, J. Electroanal. Chem. 587 (2006) 172.
[48] Y. Wang, Z.M. Sheng, H. Yang, S.P. Jiang, C.M. Li, Int. J. Hydrogen Energy 35 (2010) 10087.
[49] Y. Wang, T.S. Nguyen, X. Liu, X. Wang, J. Power Sources 195 (2010) 2619.
[50] R. Li, Z. Wei, T. Huang, A. Yu, Electrochim. Acta 56 (2011) 6860.
[51] F. Hahn, D. Floner, B. Beden, C. Lamy, Electrochim. Acta 32 (1987) 1631.
[52] F. Hahn, B. Beden, M.J. Croissant, C. Lamy, Electrochim. Acta 31 (1986) 335.
[53] I. Danaee, M. Jafarian, F. Forouzandeh, F. Gobal, M.G. Mahjani, Int. J. Hydrogen Energy 33 (2008) 4367.
[54] M. Fleischmann, K. Korinek, D. Pletcher, J Electroanal. Chem. Interfacial Electrochem. 31 (1971) 39.
[55] D.A. Corrigan, J. Electrochem. Soc. 134 (1987) 377.
[56] P.W.T. Lu, S. Srinivasan, J. Electrochem. Soc. 125 (1978) 1416.
[57] E. Laviron, J. Electroanal. Chem. Interfacial Electrochem. 101 (1979) 19.
[58] A.J. Bard, L.R. Faulkner, Electrochemical Methods. Fundamentals and Applications, second ed., John Wiley & Sons, Inc., New York, 2001.
[59] S.N. Azizi, S. Ghasemi, E. Chiani, Electrochim. Acta 88 (2013) 463.
[60] R. Ojani, J.-B. Raoof, V. Rahemi, Int. J. Hydrogen Energy 36 (2011) 13288.
[61] J.-B. Raoof, R. Ojani, S.R. Hosseini, J. Power Sources 196 (2011) 1855.
[62] I. Danaee, M. Jafarian, A. Mirzapoor, F. Gobal, M.G. Mahjani, Electrochim. Acta 55 (2010) 2093.
[63] A.A. El-Shafei, J. Electroanal. Chem. 471 (1999) 89.
[64] M. Fleischmann, K. Korinek, D. Pletcher, J. Chem. Soc., Perkin Trans. 2 (1972) 1396.
[65] R. Ojani, J.-B. Raoof, S. Fathi, Electrochim. Acta 54 (2009) 2190.
[66] M.A. Abdel Rahim, H.B. Hassan, R.M. Abdel Hamid, J. Power Sources 154 (2006) 59.
[67] Y.-Y. Yang, J. Ren, H.-X. Zhang, Z.-Y. Zhou, S.-G. Sun, W.-B. Cai, Langmuir 29 (2013) 1709.
[68] R.N. Singh, Anindita, A. Singh, Carbon 47 (2009) 271.
[69] C. Jin, X. Sun, Z. Chen, R. Dong, Mater. Chem. Phys. 135 (2012) 433.
[70] Z.-P. Sun, X.-G. Zhang, Y.-Y. Liang, H.-L. Li, Electrochem. Commun. 11 (2009) 557.
[71] K. Honda, M. Yoshimura, T.N. Rao, D.A. Tryk, A. Fujishima, K. Yasui, Y. Sakamoto, K. Nishio, H. Masuda, J. Electroanal. Chem. 514 (2001) 35.
[72] M.A. Abdel Rahim, R.M. Abdel Hameed, M.W. Khalil, J. Power Sources 134 (2004) 160.
[73] R. Pattabiraman, Appl. Catal. A: General 153 (1997) 9.
[74] R. Ojani, J.-B. Raoof, S.J. Fathi, Solid State Electrochem. 13 (2009) 927.
[75] M. Jafarian, R.B. Moghhaddam, M.G. Mahjani, F. Gobal, J. Appl. Electrochem. 36 (2006) 913.
[76] A. Ciszewski, G. Milczarek, B. Lewandowska, K. Krutowski, Electroanalysis 15 (2003) 518.
[77] A.N. Golikand, M. Asgari, M.G. Maragheh, S. Shahrokhian, J. Electroanal. Chem. 588 (2006) 155.
[78] X. Yu, P.G. Pickup, Electrochem. Commun. 11 (2009) 2012.
[79] X. Yu, P.G. Pickup, J. Power Sources 187 (2009) 493.
[80] S. Wang, A. Manthiram, Electrochim. Acta 88 (2013) 565.
[81] U.B. Demirci, J. Power Sources 173 (2007) 11.
[82] J. Greeley, J.K. Nørskov, Surf. Sci. 592 (2005) 104.
[83] B. Hammer, J.K. Nørskov, Surf. Sci. 343 (1995) 211.
[84] J.C. Davies, R.M. Nielsen, L.B. Thomsen, I. Chorkendorff, Á. Logadóttir, Z. Lodziana, J.K. Nørskov, W.X. Li, B. Hammer, S.R. Longwitz, J. Schnadt, E.K. Vestergaard, R.T. Vang, F. Besenbacher, Fuel Cells 4 (2004) 309.
[85] Z.-B. Wang, G.-P. Yin, Y.-Y. Shao, B.-Q. Yang, P.-F. Shi, P.-X. Feng, J. Power Sources 165 (2007) 9.
[86] Z.-B. Wang, G.-P. Yin, J. Zhang, Y.C. Sun, P.-F. Shi, Electrochim. Acta 51 (2006) 5691.
[87] P.K. Shen, C. Xu, R. Zeng, Y. Liu, Electrochem. Solid-State Lett. 9 (2006) A39.